Probing the distribution of ionic liquid mixtures at charged and neutral interfaces via simulations and lattice-gas theory

Takeshi Kobayashi[a],[*] Jens Smiatek,[†] and Maria Fyta[b][‡]

Institute for Computational Physics, University of Stuttgart, Allmandring 3, 70569 Stuttgart, Germany

(Dated: August 1, 2022)

Room temperature ionic liquid solutions confined between neutral and charged surfaces are investigated by means of atomistic Molecular Dynamics simulations. We study 1-Ethyl-3-methylimidazolium dicyanamide ($[EMIm]^+[DCA]^-$) in water or dimethylsulfoxid (DMSO) mixtures in confinement between two interfaces. The analysis is based on the comparison of the molecular species involved and the charged state of the surfaces. Focus is given on the influence of different water/DMSO concentrations on the microstructuring and accumulation of each species. Thermodynamic aspects, such as the entropic contributions in the observed trends are obtained from the simulations using a lattice-gas theory. The results clearly underline the differences in these properties for the water and DMSO mixtures and unravel the underlying mechanisms and inherent details. We were able to pinpoint the importance of the size and the relative permittivity of the molecules in guiding their microstructuring in the vicinity of the surfaces, as well as their interactions with the latter, i.e. the solute-surface interactions. The influence of water and DMSO on the overscreening at charged interfaces is also discussed. The analysis on the molecular accumulation at the interfaces allows us to predict whether the accumulation is entropy or enthalpy driven, which has an impact in the removal of the molecular species from the surfaces. We discuss the impact of this work in providing an essential understanding towards a careful design of electrochemical elements.

[a] Present address: Department of Chemical Engineering, University College London, London WC1E 7JE, UK

[b] Present address: Computational Biotechnology, RWTH Aachen University, Worringerweg 3, 52074 Aachen, Germany.

[*] tkobayashi@icp.uni-stuttgart.de

[†] smiatek@icp.uni-stuttgart.de

[‡] mfyta@icp.uni-stuttgart.de

I. INTRODUCTION

Room temperature ionic liquids (ILs) are tunable media that have useful applications in many novel technological applications. Hence, ILs can be considered as stable electrolytes in energy storage devices such as lithium ion batteries [1–5] up to stabilizers or destabilizers of proteins [6–13] in biotechnological applications. In order to realize such applications, the inherent properties of the ILs, meaning their interaction patterns, structural properties as well as their behavior under certain conditions have been in the focus of research in the last two decades [6, 7, 14–16]. Accordingly, bulk ILs have been investigated theoretically [17–20], computationally [7, 21–24], and experimentally [25–29]. As ILs are formed in various combinations of cations and anions of different sizes and polarities, they can also possess different properties such as conductivity, diffusivity, viscosity, volatility as well as electrochemical stability [1, 29–31], which affect the total performance of ILs in certain applications [3, 31–36]. Further modifications can be observed after the solvation of additives or impurities in combination with trace amounts of solvent molecules [31, 37–40]. Another factor influencing the IL properties and performance is the presence of interfaces (IF) and other materials such as electrodes, proteins or DNA [5, 9, 36, 39, 41–45]. For a tailor-made design of ILs in terms of certain applications, insight into their microstuctural arrangements and molecular interactions are essential.

An important example for short-range properties in ILs is the formation of layers in front of IFs. Due to electrostatic and dispersion interactions between the surfaces and the molecules, several layers parallel to the surfaces are formed on length scales of a few nanometers [46–49]. For IL mixtures including ions and other molecules, the type of solute or solvent can play a crucial role on the IL properties. Prominent examples for interfacial IL mixture effects are the accumulation of water in ILs as electrolytes for energy storage systems [50] that narrows the electrochemical stability window [51] or the stabilization of proteins in aqueous ILs [6, 7, 10–13]. Overall, the microstructure of ILs at IFs depends on the surface characteristics in terms of polarity and charge as well as the molecular properties of the individual ions in the ILs [5, 36, 42, 45, 47, 49, 52, 53]. Thus, the molecular accumulation of ions and solute species at IFs is driven by thermodynamics in combination with entropic effects for uncharged IFs [54]. In front of charged surfaces, though, the behavior of ILs is not well understood. From a theoretical point of view, the layering of dilute electrolyte mixtures in front of charged surfaces can be described by the mean-field Gouy-Chapman model [55]. As this cannot be directly applied to the case of ILs which are concentrated electrolytes, several extensions or modifications of the Gouy-Chapman theory were used [56]. Despite all changes, the presence and influence of neutral species is typically included through a background dielectric permittivity or an excluded volume consideration of voids which are not accessible by the ions [57]. Although such theories provide some insight on IL solutions, they usually ignore many essential effects like partial charges and dipolar contributions as governed by molecular details of the solution. One of the manifestations of the influence of the molecular distributions is the overscreing [58] which consists of not only double but several layers in front of the charged surfaces. The fist layer of counter ions provide excess charge to the surface charges, and the following counter-ion rich layers show oscillating charge until it converges to zero. It is widely studied theoretically [53, 57, 59, 60], experimentally[53, 61–65], and computationally [66–68]. However, the complete explanation is still far to reach and it must take atomistic details of relevant molecules including neutral species into account.

In order to study the influence of the molecular characteristics, we performed all-atom Molecular Dynamics (MD) simulations of the IL 1-ethyl-3-methyl imidazolium [EMIM]$^+$ dicyanamide [DCA]$^-$ with water or dimethyl sulfoxide (DMSO) molecules at different concentration in presence of charged interfaces. A further comparison between neutral and charged IFs reveals the contribution of the solute-surface interactions and their influence on the overall properties of these systems. A main focus is given here on the distinct features of the relevant molecules and their behavior within the IL mixtures and close to the IFs. The results from the MD simulations are further compared to a lattice-gas model [56], which describes the IL mixtures in terms of a free energy functional. We extend this theory to also include the distribution of molecules in front of the neutral surfaces.

II. METHODOLOGY

A. Simulation Details

We study in detail the microstructuring and the properties of IL mixtures confined within charged/uncharged surfaces. To this end, we perform atomistic Molecular Dynamics (MD) simulations for distinct IL solutions with either water or dimethyl sulfoxide (DMSO). We choose water as a representative protic solute and DMSO as a representative aprotic solute. The description of assignment of DMSO or water as a solute, co-solvent or solvent depends on the concentration, such that low molar concentration refers to solute properties while high molar concentration relates DMSO or water being the solvent. In order to simplify the following discussion, we use the term 'solute' for either DMSO or water independent of the actual concentration. For the IL, we consider 1-ethyl-3-methylimidazolium dicyanamide
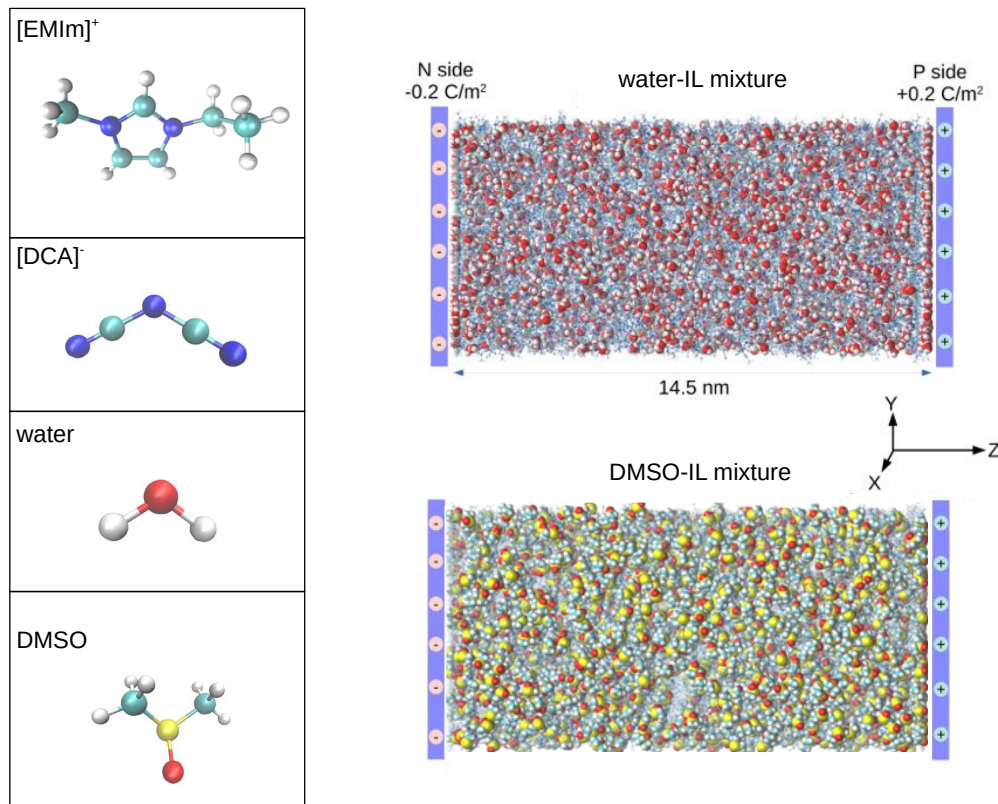
FIG. 1: Left: ball & stick models of the IL ([EMIm]$^+$ cations and [DCA]$^-$ anions), as well as water and DMSO molecules. Right: a snapshot of an equilibrated IL-mixture with water (top) and DMSO (bottom) between two charged surfaces at a solute concentration of $x_{\rm sol} = 0.500$. The axes, the charge on the IFs, and the distance between the IFs are depicted. 'N side' and 'P side' denote the negatively and positively charged IF, respectively. The hydrogen, oxygen, nitrogen, carbon, sulfur atoms are shown in white, red, blue, gray, and yellow, respectively.

[EMIm]$^+$[DCA]$^-$, at various solute (water or DMSO) mole fractions ranging from $x_{\rm sol} = 0$ (pure IL) to $x_{\rm sol} = 0.875$ (highly diluted IL solution). Specifically, solute mole fractions of $\{0, 0.125, 0.250, 0.375, 0.500, 0.625, 0.75, 0.875\}$ were simulated. The geometries of all species, ions and molecules, are shown in Fig. 1 together with snapshots of the IL mixtures between the two interfaces.

The atomistic MD simulations with the GROMACS 5.1.3 software package [69–71] rely on the OPLS/AA force fields for the ions and DMSO [72–75] and the SPC/E model for water [76]. This combination has already been validated for water-IL mixtures [54, 77]. In all simulations, the temperature was set to T = 300 K by an improved velocity-rescaling thermostat [78], using a coupling time constant of 0.1 ps. Electrostatic interactions were treated through the particle mesh Ewald (PME) method [79, 80], where a real-space cutoff of 1.0 nm and a grid spacing of 0.16 nm with a fourth-order interpolation scheme were used. The Lennard-Jones (LJ) interactions were truncated at 1.0 nm and shifted to zero. The equations of motion were integrated using the Leapfrog algorithm with an elementary time step of 2 fs. All bonds were constrained by the LINCS algorithm [81]. An energy minimization was first performed using a conjugate-gradient method, followed by an equilibration period of 10 ns under constant volume and constant temperature (NVT) conditions, and a subsequent equilibration run of 10 ns under constant temperature and constant pressure (NpT) conditions. The final (NpT) production runs were performed for 300 ns each. Atomic positions and velocities were stored every 10 ps. We have used computational boxes of dimensions 6.3 nm - 6.5 nm in the periodic x, y directions and fixed the length z = 14.5 nm in the z direction perpendicular to the surfaces. These were placed at z = 0 nm and z = 14.5 nm in parallel to the xy plane (see Fig.1 for the definition of axes and dimensions). All species were randomly inserted using the software package PACKMOL [82]. The corresponding numbers of molecules and ions for the respective mole fractions are shown in Table I. In order to compensate periodic interactions in z-direction, a 3D-Ewald summation method with an electrostatic gap correction term [83] was used, thereby assuming empty boxes with a height of three times the box length. We performed two types of simulations, one with the IL mixtures confined between uncharged IFs and one with the IL mixtures within charged IFs. For the charged surfaces, the surface charge is implemented by image charges on the surfaces so that the absolute value of the charge density

TABLE I: The input parameters for the MD simulations of water-[EMIM]$^+$[DCA]$^-$ mixtures and DMSO-[EMIM]$^+$[DCA]$^-$ mixtures. 'NCF' and 'CIF' refer to the neutral and charged IFs, respectively.

Mixture	Mole fraction of solvent x_{sol}							
	0	0.125	0.250	0.375	0.500	0.625	0.750	0.875
water-[EMIM]$^+$[DCA]$^-$								
Number of ions N_i	2500	2310	2257	2187	2090	1946	1710	1254
Number of solutes N_{sol}	0	330	752	1312	2090	3243	5130	8778
Box length in x/y directions (nm) (NIF)	6.82	6.61	6.61	6.60	6.58	6.56	6.53	6.46
Box length in x/y directions (nm) (CIF)	6.78	6.57	6.57	6.56	6.55	6.54	6.51	6.46
DMSO-[EMIM]$^+$[DCA]$^-$								
Number of ions N_i	2500	2310	2190	2000	1760	1422	1110	640
Number of solutes N_{sol}	0	330	730	1200	1760	2370	3330	4480
Box length in x/y directions (nm) (NIF)	6.82	6.76	6.83	6.86	6.87	6.77	6.93	6.99
Box length in x/y directions (nm) (CIF)	6.78	6.72	6.80	6.82	6.83	6.75	6.92	7.00

equals approximately 0.2 C/m^2. The image charges can move on the surface which allows us to include the influence of the fluctuation of the change distribution on the surfaces. This is essential to describe the correct properties of the system [68]. The left and right surfaces reveal negative and positive charges, respectively (see Fig.1). The pressure was kept constant at p = 1 bar by a semi-isotropic Parrinello–Rahman barostat [84] (periodic x- and y-dimensions with a fixed z-dimension) with a coupling time constant of 2 ps and a compressibility of 4.5×10^{-5} bar^{-1}.

B. Lattice-gas model and free energies

In order to calculate chemical potentials of the species in the mixtures and the entropic contributions to them, we briefly introduce the lattice-gas model [56] for both neat ILs, as well as IL mixtures which is used to study the outcomes of the simulations. In this framework, the system is sliced into slabs parallel to the xy plane as depicted in Fig.2 in two-dimensions. These slabs are in turn divided into sites, which can be occupied by the molecular species, namely the cations, the anions, and the solute molecules. We next describe the derivation of thermodynamic observables based on this model:

a. Neat ILs: the free energy F of IL mixtures is given through

$$F = e\Phi(N_+ - N_-) + B_+ N_+^2 + B_- N_-^2 + C N_+ N_- - k_B T \ln W , \qquad (1)$$

where e the elementary charge, Φ the mean field electrostatic potential, N the number of the total available sites for each species within the slab parallel to the xy plane, N_+ and N_- the numbers of cations and anions, respectively, B_+ and B_- and C the coefficients for the cation-cation, anion-anion and cation-anion interactions, T the temperature, k_B the Boltzmann constant, and $k_B \ln W$ the mixing entropy of the mixture. The latter can be expressed as

$$S = k_B \ln W = k_B \ln \frac{N!}{(N - n_+ N_+ - n_- N_-)!(n_+ N_+)!(n_- N_-)!}, \qquad (2)$$

where k_B is the known Boltzmann constant and N the number of the total available sites for each species within the slab parallel to the xy plane, and n_+ and n_- are the number of the sites occupied by a cation and an anion, respectively.

b. IL mixtures The lattice-gas theory was originally developed for dilute electrolytes, but can be extended to neutral mixtures [57]. For the latter, the free energy F of the IL mixtures is described through

$$F = e\Phi(N_+ - N_-) + \sum_i (U_i^{\text{IF}} N_i) - \vec{d} \cdot \vec{E} N_s + B_+ N_+^2 + B_- N_-^2 + B_s N_s^2 + \sum_i \sum_{i \neq j} C_{ij} N_i N_j - TS, \qquad (3)$$

with $(i, j = +, -, s)$. The subscript s denotes the solute, N_s is the number of solutes, $\vec{d}$ is the mean dipole moment of the solute molecules, B_s is the coefficient for the solute-solute interactions, C_{ij} the coefficient for the interaction of molecules i and j, and $\vec{E}$ is the mean electric field applied on the system. The interaction energy (U_i^{IF}) between a
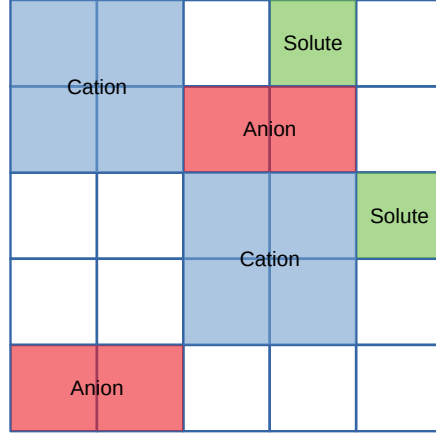
FIG. 2: A schematic view of the concept behind the lattice-gas model representing the slicing of the slab of a mixture on a two-dimensional xy plane. The slab is divided into a lattice, on which the various molecular species occupy different sites depending on their molecular size as denoted by the different colors and labels.

molecule of species i with the surface was added to express the non-Coulomb interactions between all species in the solution and the surface. The entropy is now given as

$$S = k_B \ln W = k_B \ln \frac{N!}{(N - n_+ N_+ - n_- N_- - n_s N_s)!(n_+ N_+)!(n_- N_-)!(n_s N_s)!}, \tag{4}$$

where, in addition to the notations used in Eqn.(2), n_s is the number of the sites occupied by a solute molecule.

The free energies in Eq.3 provide access to other thermodynamic properties such as the chemical potentials relevant to the mixtures and the contributions of entropy and enthalpy. The chemical potentials of the molecular species can be calculated from the derivatives of the free energy with respect to the number N_i of each species using the Stirling formula ($\ln N! \approx N \ln N + N$) leading to the expressions

$$\mu_+ = \left(\frac{\partial F}{\partial N_+}\right)_{T,V} = e\Phi + U_+^{\text{IF}} + 2B_+ N_+ + C_{+-} N_- + C_{+s} N_s - k_B T \ln \frac{n_+ N_+}{N - n_+ N_+ - n_- N_- - n_s N_s} \tag{5}$$

$$\mu_- = \left(\frac{\partial F}{\partial N_-}\right)_{T,V} = -e\Phi + U_-^{\text{IF}} + 2B_- N_- + C_{+-} N_+ + C_{-s} N_s - k_B T \ln \frac{n_- N_-}{N - n_+ N_+ - n_- N_- - n_s N_s} \tag{6}$$

$$\mu_s = \left(\frac{\partial F}{\partial N_s}\right)_{T,V} = -\vec{d} \cdot \vec{E} + U_s^{\text{IF}} + 2B_s N_s + C_{+s} N_+ + C_{-s} N_- - k_B T \ln \frac{n_s N_s}{N - n_+ N_+ - n_- N_- - n_s N_s} \tag{7}$$

where μ_i with $i = +, -, s$ represents the chemical potential of the cation, anion, and solute molecules, respectively. One usually employs the indistinguishable ion approach [7] for reasons of thermodynamic consistency. However, referring to individual ion species is convenient for evaluating the detailed thermodynamic quantities from simulation results. In a system in equilibrium, the chemical potentials of each species and at each position are identical. Hence, by equating the chemical potential in bulk solution μ_i^{bulk} and at the IF μ_i^{IF}, setting the interaction term $2B_i N_i + \sum_{j \neq i} C_{ij} N_j = E_i$ with the intermolecular interaction energy E_i, and using the relations $\Phi = 0$, $\vec{d} \cdot \vec{E}^{\text{bulk}} = 0$ and $U^{\text{IF}} = 0$ in bulk, we are led to the following equations:

$$\Delta H_+ - T\Delta S_+ = (E_+^{\text{bulk}} - E_+^{\text{IF}}) - e\Phi^{\text{IF}} - U_+^{\text{IF}} - k_B T \ln \frac{N_+^{\text{bulk}} \cdot (N - n_+ N_+^{\text{IF}} - n_- N_-^{\text{IF}} - n_s N_s^{\text{IF}})}{N_+^{\text{IF}} \cdot (N - n_+ N_+^{\text{bulk}} - n_- N_-^{\text{bulk}} - n_s N_s^{\text{bulk}})} \tag{8}$$

$$= 0,$$

$$\Delta H_- - T\Delta S_- = (E_-^{\text{bulk}} - E_-^{\text{IF}}) + e\Phi^{\text{IF}} - U_-^{\text{IF}} - k_B T \ln \frac{N_-^{\text{bulk}} \cdot (N - n_+ N_+^{\text{IF}} - n_- N_-^{\text{IF}} - n_s N_s^{\text{IF}})}{N_-^{\text{IF}} \cdot (N - n_+ N_+^{\text{bulk}} - n_- N_-^{\text{bulk}} - n_s N_s^{\text{bulk}})} \tag{9}$$
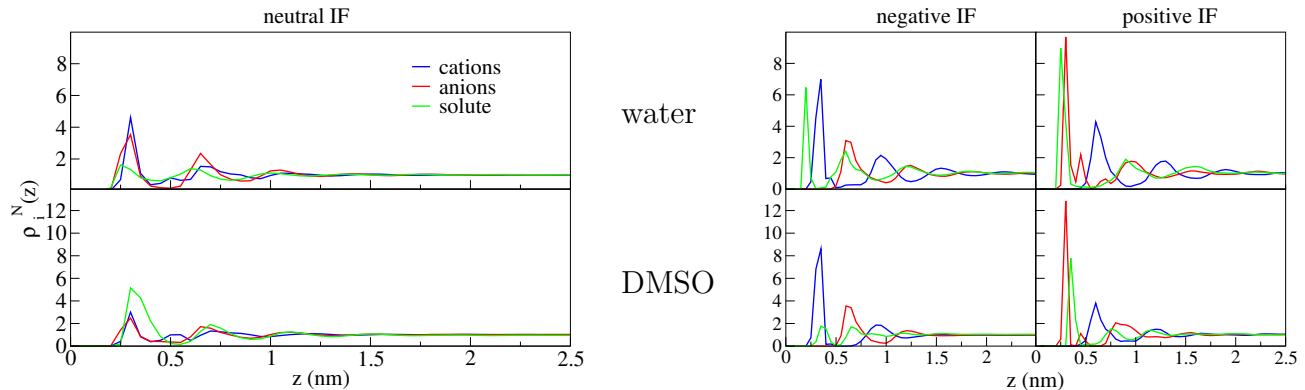
$$= 0,$$

FIG. 3: The normalized molecular density $\rho_i^N(z)$ of each species at a solute concentration of $x_{\text{sol}} = 0.5$ for (top) water and (bottom) DMSO mixtures with respect to the distance from the IF. The results are shown for neutral (left) and (right) charged surfaces as indicated by the labels. In the left panel due to the symmetric configuration for neutral surfaces only one is shown located at $z=0$ nm. The coloring of the lines corresponds to the species given in the legend.

$$\Delta H_s - T\Delta S_s = (E_s^{\text{bulk}} - E_s^{\text{IF}}) + \vec{d} \cdot \vec{E}^{\text{IF}} - U_s^{\text{IF}} - k_B T \ln \frac{N_s^{\text{bulk}} \cdot (N - n_+ N_+^{\text{IF}} - n_- N_-^{\text{IF}} - n_s N_s^{\text{IF}})}{N_s^{\text{IF}} \cdot (N - n_+ N_+^{\text{bulk}} - n_- N_-^{\text{bulk}} - n_s N_s^{\text{bulk}})} \quad (10)$$

$$= 0,$$

where ΔH_i and ΔS_i with $i = +, -, s$ are the enthalpic and entropic contributions to the free energy for cations, anions, and solutes, respectively. These contributions are related to the change in the chemical potentials in the solutions at IFs compared to bulk solutions. In terms of the previous expressions, it is possible to use the results from the simulations in order to calculate all energetic contributions and evaluate the behavior of each species at the IFs. In these calculations, the bulk solutions are taken as the reference. Accordingly, we use the lattice-gas theory together with the data from our simulations in order to access the microscopic details of the IL mixtures close to neutral and charged IFs.

III. RESULTS

A. Density profiles at the interfaces

We start our analysis with the normalized molecular density profiles of each species in the solution mixtures, as directly obtained from the MD simulations. The normalized molecular density denoted as $\rho_i^N(z)$ is the local density at the position z (perpendicular to the IFs) divided by the bulk density. The density is calculated with respect to the center of mass of each molecule and is given as a function of the distance z connecting the two interfaces (see axes in Fig.1). According to this definition, $\rho_i^N(z)$ converges to unity in the bulk near the center of the simulation box. Both in front of charged and neutral surfaces, experimental results provided some evidence for the formation of distinct layers [85]. A representative example for the layering in front of the neutral IFs for $x_{\text{sol}} = 0.5$ in terms of water and DMSO mixtures is shown in Fig.3(left). A more detailed inspection of these results highlight that in both cases three distinct layers are formed. The intensity of the peak for the solutes is about 3 times larger for DMSO compared to the protic water molecules. Accordingly, the ions show a reversed behavior in presence of both solutes. The first peak is located at $z_1 = 0.3$ nm for the cations and anions, at $z_1 = 0.25$ nm for water, and at $z_1 = 0.3$ nm for DMSO.

In order to evaluate the difference in the accumulation of the species close to charged IFs, we follow the same procedure as discussed above. The respective results for the IL mixtures and both the negatively and positively charged interfaces are depicted on the right of Fig.3 again for a solute concentration of $x_{\text{sol}} = 0.5$. The layering here differs from the case of the neutral IFs, as the position of the peaks shift to $z_1 = (0.3 - 0.35)$ nm for the cations, 0.3 nm for anions, 0.2 nm for water, and 0.4nm for DMSO close to the negative IF, and 0.3 nm for DMSO close to the positive IF. In the case of charged IFs, the relative heights of the first layer for all species shows the opposite trend compared to the neutral IFs. Our results depict the formation of electric double layers (EDLs) [56, 86], which include the counterion-rich layer in front of the surface and the following co-ion layer in front of both negatively and
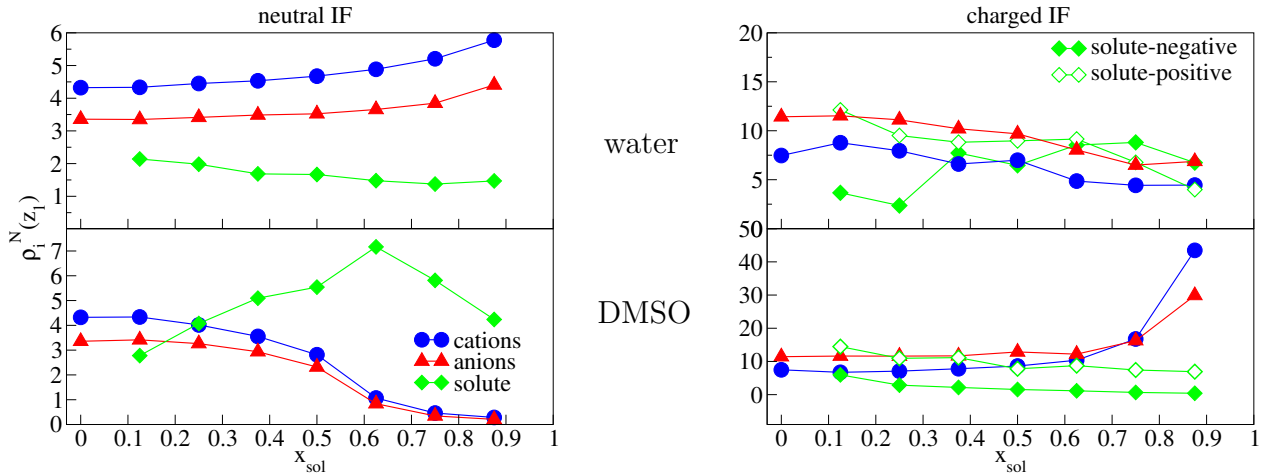
FIG. 4: The normalized number density $\rho_{\mathrm{sol}}^N(z_i)$ of each species within the first layer with respect to different solute concentration x_{sol} for (top) water and (bottom) DMSO mixtures with respect to the distance from the IF. The results are shown for neutral (left) and charged (right) surfaces as indicated by the labels. In the left panel due to the symmetric configuration for neutral surfaces only one is shown located at $z=0$ nm. The coloring of the lines corresponds to the species given in the legend.

positively charged surfaces. The polar water molecules are accumulated closer to both IFs, followed by the cations close to the negative IF and the anions close to the positive IF. The water molecules are much smaller than DMSO and have a higher relative permittivity, such that they can occupy the voids between the ions and reveal favorable electrostatic interactions which rationalizes the higher water concentration in the EDL. In the DMSO mixtures, the DMSO molecules form the second layer in front of the charged IFs, following the cations close to the negative IFs and the anions close the positive IF. The layers extend further towards the bulk, while at the charged IFs roughly six layers are formed for mixtures including water in contrast to four layers in presence of DMSO.

The positions of the peaks from the normalized molecular densities in Fig.3 are further used for the calculation of the normalized number density $\rho_{\mathrm{sol}}^N(z_1)$ of each species within the first layer at z_1 close to each IF. The results with respect to the solute concentration x_{sol} are depicted in Fig.4(left). A clear difference can be seen in the water and DMSO mixtures for both neutral and charged IFs. In water mixtures, the number of ions increases in the first layer with an increasing concentration x_{sol}, while for DMSO the number of ions, both for cations or anions decreases. For increasing solute concentrations, the number of water molecules within the first layer close to the IFs slightly decreases. For the DMSO mixtures, the number of DMSO molecules increases up to a mole fraction of $x_{\mathrm{sol}} = 0.625$ and then drop. Accordingly, comparing water and DMSO mixtures underlines a reversed behavior in terms of the accumulation of each species within the first layer close to neutral IFs. This is a direct consequence of the different solute type, its size and electronegativity and can be rationalized by entropy-driven effects [54].

For charged IFs as shown on the right of Fig. 4, the accumulation of molecular species closest to the IFs reveals some differences when compared to uncharged IFs. Increasing the solute concentration x_{sol} leads to a decrease of the number of ions in front of the charged surfaces in the water mixtures and a significant increase at $x_{sol} = 0.75$ for the DMSO mixtures. Regarding the solute accumulation, in water this is enhanced at the positive side up to a concentration of $x_{\mathrm{sol}} = 0.875$ and is depleted at the negative side of the IFs. DMSO is depleted both at the negative and positive IFs. The higher accumulation of the water molecules close to the positive IF is probably related to the high dipole moment in the direction of the negatively charged oxygen atom which does not lower the conformation entropy. In contrast, the reverse arrangement results in restricted rotational movements, such that the entropic contribution is reduced which rationalizes the lower occurrence probability of water in front of negatively charged IFs. The distinct accumulation behavior between water and DMSO is crucial for practical applications of IL mixtures in terms of electrochemical stabilities [36], which rely on the type of species, ions or solutes, that are preferably accumulated at IFs.

B. Entropy and molecular accumulation

Our results have underlined a distinct accumulation behavior of the molecular species at the IFs. In order to provide insight into the fundamental mechanism of this accumulation, we calculate the entropic contribution to the chemical

potentials as provided in Eqs. 9, 10, 11. For each species at different solute concentrations, we first need to estimate

$$\frac{n_i N_i}{N - n_+ N_+ - n_- N_- - n_s N_s} = \frac{\rho_i v_i / a_i}{1.0 - \rho_+ v_+ / a_+ - \rho_- v_- / a_- - \rho_s v_s / a_s}, \tag{11}$$

according to Eqs.6, 5, 7, where ρ_i is the atomic number density of species $i = +, -, s$ in combination with the molecular volume, v_i, which is $v_+ = 0.116$ nm^3 for the cations, $v_+ = 0.0553$ nm^3 for the anions, $v_s = 0.0196$ nm^3 for water, and $v_s = 0.0717$ nm^3 for DMSO as obtained from the literature [87]. The number of atoms in each species, a_i, is $a_+ = 19$ for the cations, $a_- = 5$ for the anions, $a_s = 10$ for DMSO, and $a_s = 3$ for water. Using Eq.11, the entropic term $-k_B T \Delta S_i$ in Eqs.9, 10, and 11 is shown in Fig.5 (left) for neutral surfaces at distances in the range 0.125 nm – 0.375 nm from the position of the IFs. These distances include the first peaks of the normalized molecular densities as discussed above. Specifically, in water mixtures a higher entropy term when compared to the solute can be observed for the ions. For DMSO mixtures, a higher entropy term can be associated with the DMSO molecules. These trends in both types of mixtures follow those for the normalized molecular densities in Fig.3(left). Our results underscore the fact that the change in the accumulation behavior of molecules is governed by changes in the entropy. Accordingly, at neutral IFs, the accumulation of the molecular species close to the IFs is entropy driven in agreement with previous findings [54].

Next, we compare these results to the respective ones for the IL mixtures at the charged IFs. The outcomes are depicted in Fig.5 (right). Similar trends as for the neutral IFs can be observed in the DMSO mixtures and only for the anions in water mixtures, as for these the entropy term increases with the solute concentration as in the case of the neutral IFs. The other species in water mixtures show a distinct behavior, as their trends are on average reversed when compared to the neutral IFs. A comparison with the respective normalized molecular densities in Fig.3(right) reveals the correlation of a higher accumulation as indicated by the high peak in the densities to a lower entropy contribution. In more detail, in water-IL mixtures, the accumulation of species decreases with the following order: water at negative IFs, water at positive IFs, and ions. At the same concentration of $x_{\text{sol}} = 0.5$, the entropy contribution decreases with the following order: ions, water at positive IFs, and water at negative IFs. In DMSO-IL mixtures, the trends at the same concentration of $x_{\text{sol}} = 0.5$ as in Fig.3(right) show a stronger accumulation of the ions at the charged IFs, followed by the DMSO molecules at positive and negative IFs, respectively. A comparable trend is observed for the entropic contributions within the DMSO mixtures.

Overall, our observations point to distinct changes in the entropy contribution in the water accumulation in front of charged IFs when compared to DMSO mixtures. These results highlight the fact that the differences in the accumulation of the species is driven by entropic effects, larger contributions in terms of electrostatic and dipolar interactions affect the free energy in presence of charged interfaces which rationalizes the differences in our observations. In the end, adding a solute with low permittivity like DMSO does not change the molecular structuring at IFs, while a solute with high permittivity like water considerably changes the structuring by interacting strongly with the ions and aligning favorably its orientation with the charged IF. Note, that the experimental values of the relative permittivity of water and DMSO are 78.42 and 46.64 at 297.15 K [88], and the corresponding values calculated by our simulations using the dipole moment fluctuation formula [89] are 71.14 and 44.40, respectively. These results are important and striking as they unravel the underlying mechanism of the interaction of molecular species with interfaces, allowing a proper selection of the species type in order to tune their interaction, thus their accumulation at the IFs.

C. Molecular specifics: dipole moments and interactions with surfaces

Our previous results clearly underline the important role of the solute molecules in defining the behavior of the IL mixtures especially in front of the charged IFs. In order to obtain a deeper insight into the distinct features that the specific choice of molecular species can offer, we turn to the solute-surface interactions $\vec{d} \cdot \vec{E}^{\text{IF}}$ in Eq.11 and summarize the results in Fig.6. At a first glance, the solute-surface interactions are of the same order apart from the water negative-surface interactions which are 2-4 times stronger. This observation can be understood with regard to the higher relative permittivity of water when compared to DMSO molecules in combination with the weak interaction between cations and water [24]. As observed above, in the case of water mixtures Fig.3, the water molecules are closest to the negative IF, followed by the cations. Accordingly, water molecules can strongly interact with the external field, namely the electrostatic field generated by the surface charge. At the positive IF, though the water molecules are again closest to the surface, these are also more closer to the anions. As a result, the water molecules do not only interact with the IF, but also with the neighboring anion layer. In the case of DMSO mixtures, the solute-surface interactions at the negative IF are less strong than the water mixtures due to the lower relative permittivity of DMSO. In consequence, DMSO is more restricted in the spatial conformations in order to maximize its interactions with the charged interface. At the positive IF, the solute-surface interactions are about two times stronger, as the anion layer between the surface and DMSO enhances these interactions.
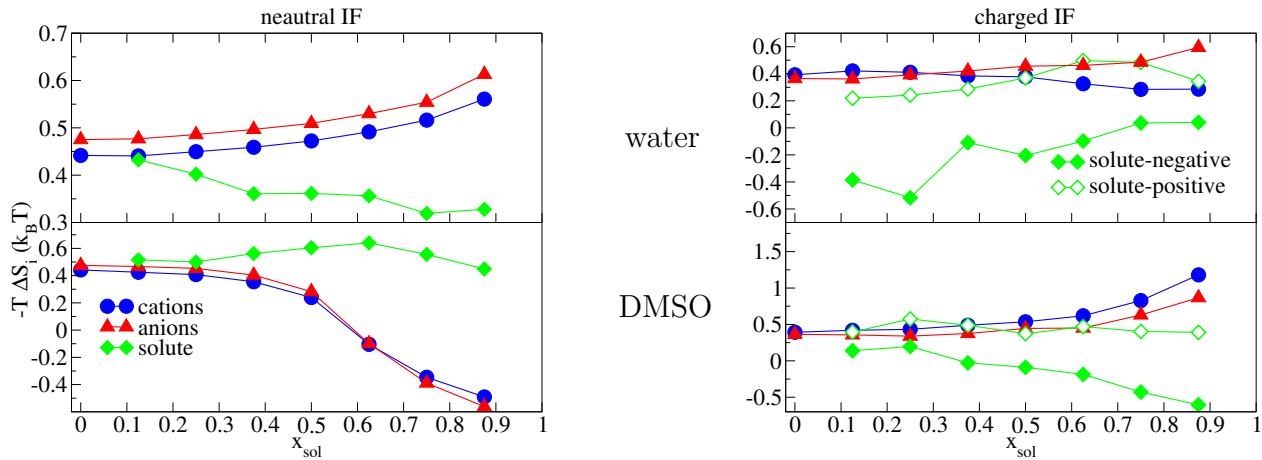
FIG. 5: The entropy term at the first layer with respect to the solute concentration for (left) the neutral and (right) the charged IFs and (top) the water and (bottom) the DMSO mixtures, respectively. The symbols and coloring for the species follows the legend. For the charged IFs (right), filled and open symbols refer to the solute interactions with the negative and positive IF, respectively.
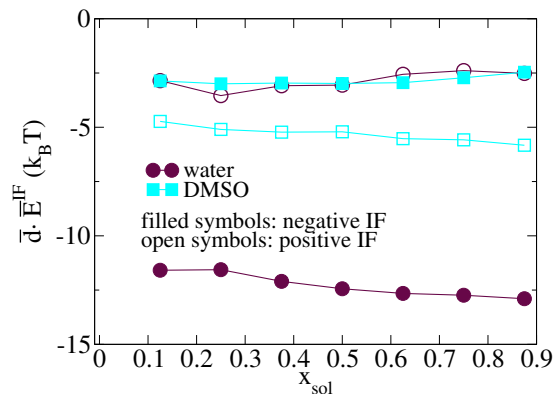

FIG. 6: The solute-surface interactions for the charged IFs and the IL mixtures at different solute concentrations. The symbols for the solutes correspond to the legend. Filled and open symbols refer to the solute interactions with the negative and positive IF, respectively.

In order to analyze further the influence of the surface, we access the average normalized dipole moment of solutes. Due to the symmetric configuration along the x, y directions, we only focus on the z component of the average dipole moment of the solutes with respect to their distance from the surface, which is given through:

$$\overline{d_z(z)} = \frac{1}{N} \sum_i \frac{\mu_{z,i}(z)}{|\vec{\mu}|}, \tag{12}$$

where $\mu_{z,i}$ is the z component of the dipole moment of the solute i, and $|\vec{\mu}|$ is the norm of the dipole moment of the solute, which is 2.35D for water and 4.416D for DMSO as calculated from the simulations. Note, that the respective experimental values are 3.960D for DMSO and 1.855D for water [90]. The sum is taken over all N solute molecules located at the distance z from the surface. Our results shown in Fig.7 reveal that, even in front of the neutral surfaces, the periodic orientational preference of solutes is observed. In water mixtures at neutral IFs, the first peak at $z = 0.2$ nm, corresponds to a positive average dipole moment for water up to a solute concentration of $x_{sol} = 0.750$. At this latter concentration, the first peak is shifted to $z = 0.15$ nm and corresponds to a negative value for the average dipole moment of water which shows that the O-H bonds of the water molecules are directed towards the surface. This change indicates that the strong interaction of the hydrogen atoms of water with the anions is important up to high concentrations [24]. In the case of DMSO mixtures at neutral surfaces, no modifications for DMSO can be observed, as DMSO interacts mostly through van der Waals interactions with other molecules. These interactions are not highly influenced by changes in the solute concentration [24].
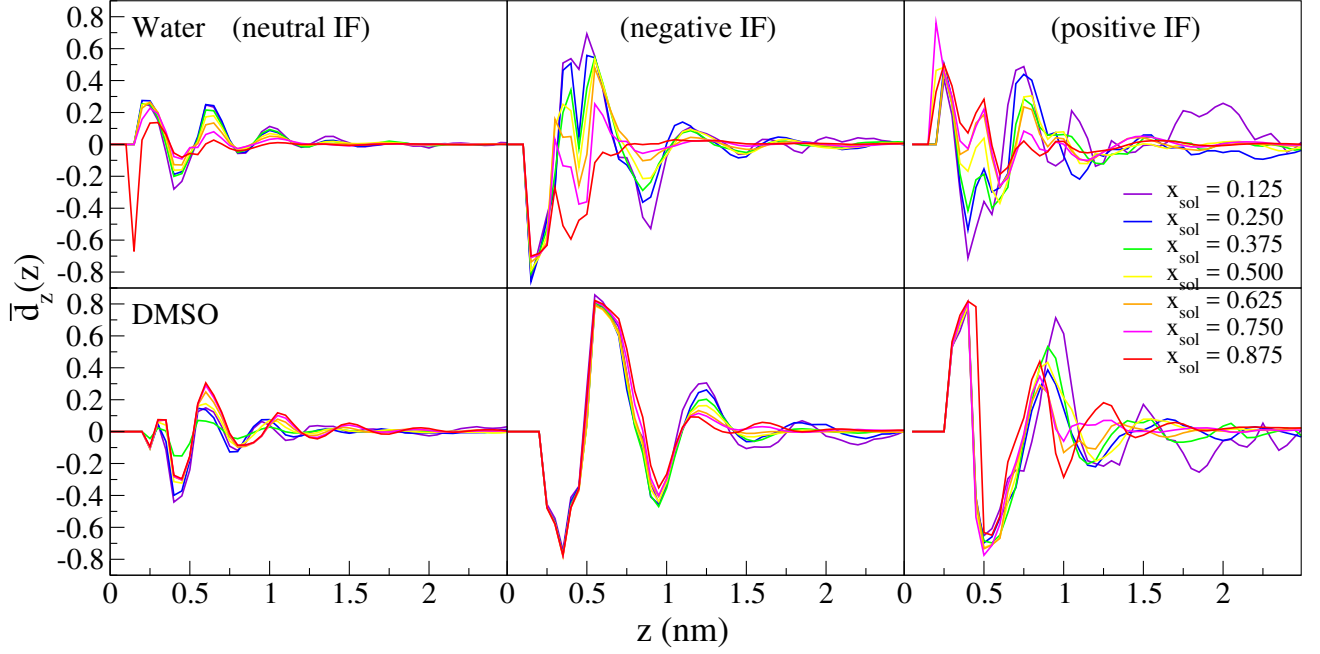
FIG. 7: The z component of the average dipole moment $\overline{d_z(z)}$ of solutes in front of (left) neutral, (middle) negatively and (right) positively charged surfaces at different solute concentrations. The color convention for the different $x$sol is denoted in the legend.

In front of charged surfaces, the amplitude of the average normalized dipole moments is enhanced compared to the neutral surfaces. As observed in Fig.3, the main differences between neutral surfaces and charged surfaces is the existence of the cation rich layer in front of the negatively charged surface and the anion rich layer in front of the positively charged surface. For a lower water concentration, the water dipole moments point to the surface due to the strong electric field between the cation-rich layer at $z = 0.3$ nm and the anion rich layer at $z = 0.6$ nm. At a high water concentration of $x_{\mathrm{sol}} = 0.875$, the dipole moments of water molecules are oriented towards the surface as water due to its small size can fill the gaps between the ion layers and clusters at the interface. At the negative IF, significant variations in the second peak ($z = 0.4 \sim 0.6$ nm) of the average normalized dipole moments can be observed when increasing the water concentration. Close to the positive IF, the water molecules interact with the anions at low water concentrations. We have observed at high water concentrations, that water starts to form again clusters and hydrogen bonded networks. This observation is highly relevant to the interaction energy between the surface and the solute U_s^{IF} and $\vec{d} \cdot \vec{E}^{\mathrm{IF}}$ in Eq.11 and reveals that the electrostatic contribution from the interface $\vec{d} \cdot \vec{E}^{\mathrm{IF}}$ is important only in the case of charged surfaces as expected. It strongly influences the structuring of the ions in front of the charged surfaces, enhancing the differences in the solute-surface interactions for the positively and negatively charged surfaces as observed in Fig.6. In DMSO mixtures close to the positive IF, the DMSO concentration has an evident effect due to the weak interactions between anions and DMSO. Accordingly, there is a higher response to the external electrical field. In front of the negatively charged surface, the DMSO mixtures do not show any significant changes with increasing DMSO concentration. DMSO is depleted from the IF as shown in Fig.3 and the structuring of the ions at the IF is not strongly affected by changes in the DMSO concentration.

D. Overscreening at the interfaces

Finally, the influence of solute molecules on overscreening effects is analyzed. First, in order to observe the overscreening at the IFs, the cumulative charge $Q(z)$ with respect to the distance z from the negative IF and the positive IF in the water and DMSO mixtures using the following equation
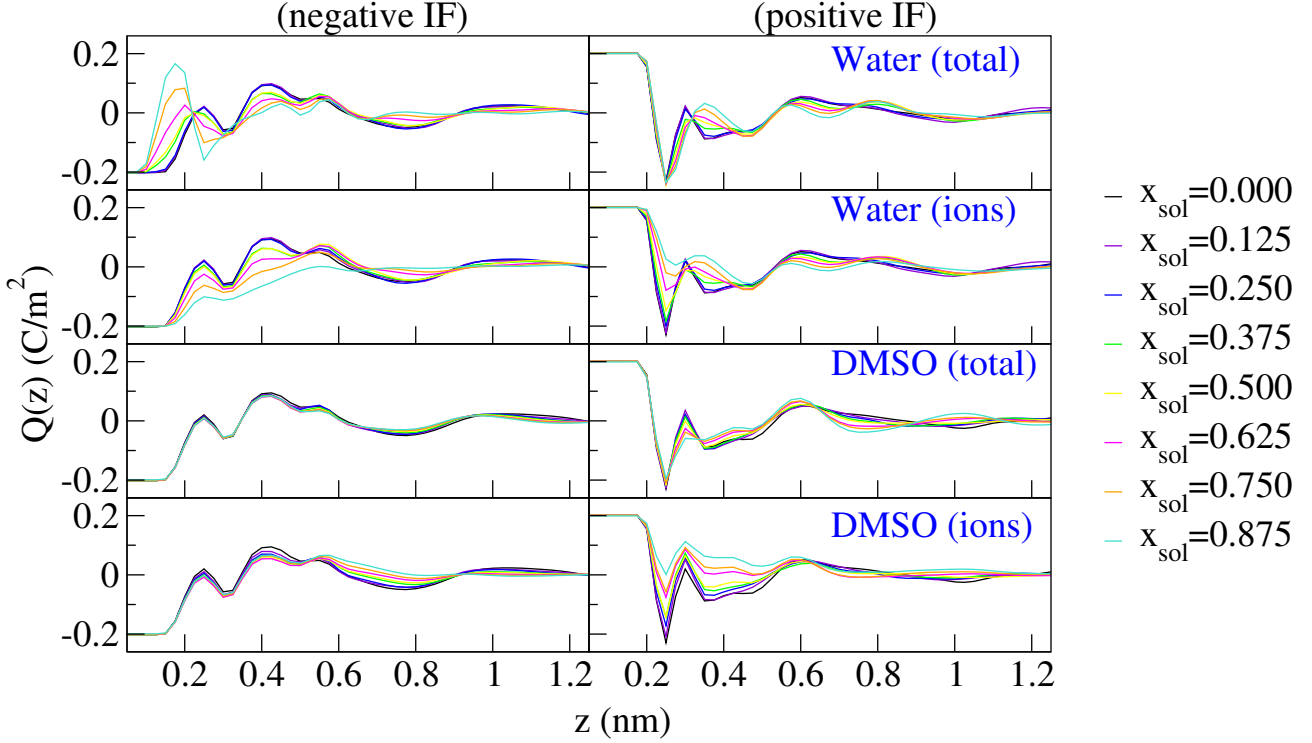
FIG. 8: The cumulative charges $Q(z)$ with respect to the distance z from negative surfaces (left panels) and positive surfaces (right panels). From the top to the bottom: the contributions from all the species in the water mixtures (top row), the ions in water mixtures (second row), the total contribution from all the species in the DMSO mixtures (third row), and the ions in the DMSO mixtures (bottom row).

$$Q(z) = \int_0^z q(z)dz, \tag{13}$$

where z is the distance from the surface and $q(z)$ is the charge density at distance z. In order to relate the accumulation of each species at IFs with the overscreening, the contribution of total species and ions, both of which include the surface charges, are calculated separately. The calculated values are shown in Fig. 8.

Interestingly, except for the water mixtures at negative IF, adding solutes does not affect the total screening at the highest peaks (located at 0.4 nm at negative IF and 0.25 nm at positive IF) shown in the top and the third rows in Fig. 8. Note that, overscreening occurs when $Q(z) > 0$ at the negative IFs and $Q(z) < 0$ at positive IFs. In the water mixtures at negative IF where water interacts very weakly with cations, the highest peak position shifts to around 0.18 nm due to the accumulation of the water molecules. The contributions from ions (the second and the bottom rows in Fig. 8) decrease with respect to the solute concentration due to the decrease of the concentration of ions. An exception is the case of DMSO mixtures at the negative IF, where the DMSO is depleted from the IF and the contributions from ions remain dominant. Combining these observations underlines that the total screening is determined by the combination of the surface charge, the shape of cations and anions of IL, and the interaction between the solute and the ILs at IFs. However, the screening does not depend on the distribution of molecules at the IFs. Note, that weak interactions between ILs and the solute at IFs and the small size of the solute molecules can change the amount of overscreening effects. This finding is consistent with dipole-surface interactions at the negative IF in the water mixtures discussed in the previous section, where the strong adsorption of water to the negative surface charge is observed.

IV. CONCLUSIONS

We have studied confined water-[EMIm]$^+$[DCA]$^-$ and DMSO-[EMIm]$^+$[DCA]$^-$ mixtures using atomistic MD simulations. The confinement is imposed by two neutral or oppositely charged structureless walls with a surface charge of $0.2C/m^2$. The influence of different water/DMSO concentrations on the microstructuring, accumulation and thermodynamics of each species is discussed. For the latter, the contribution of the entropy directly from the simulation results using a lattice-gas theory is evaluated. Our work clearly underlines the differences between water-IL and DMSO-IL mixtures. The results indicate that the differences in microstructuring of the molecular species in front of both neutral and charged surfaces are governed by entropy changes throughout the solute concentration range. An exception from this trend was clear for water in front of the positively charged surface, where the strong interaction between anions and water play an important role suppressing the interaction of water with the positively IF. We have provided a direct insight to IL mixtures confined between surfaces, through a detailed analysis of their structural and dielectric characteristics. We were able to connect our observations to the explicit solute-surface interactions in the confined IL mixtures and underline their inherent differences. The investigation of these, revealing the significant role of the interaction between the surface charge and the dipole-moment of solutes, pointed to the observations that water reacts to the surface charge of the negatively charged surface, while DMSO reacts less strongly to the surface charge of the positively charged surface.

In view of practical applications, the different trends in the IL mixtures including water or DMSO, provide an essential understanding which stimulates further research in improved electrochemical devices. Our results reveal that the removal of water from the surface is a challenging task due to the small size of the molecule. Water is a molecule with high electronegativity, which interacts more strongly with the anions than with the positive IFs [91–93]. This shielding effect may protect water from direct surface electrolysis which allows to increase the operating voltage of the device. Alternatively, using ions with higher electronegativity lead to weaker interactions with the water molecules in addition to the ionic shielding effect [92, 93], such that water removal from the charged interfaces might be enhanced. Overall, our results clearly show that the use of a large solute in combination with large ions can suppress the accumulation of solute molecules in front of charged surfaces. Through this choice, the interactions between surface charges and the solutes during the dilution of ILs can be prevented. Alternatively, solutes interacting strongly with ions can be chosen in order to reduce the interactions between surfaces and the solutes as also observed in the opposite case to our system [53], where water strongly interacts with cations at negative IFs. This is an important aspect for the chemical stability of IL mixtures when adding solutes in order to increase their conductivity. In the end, our study provides valuable insight into the proper choice of the molecule type and size in tailoring the cation-anion combination in IL mixtures for specific purposes and applications.

ACKNOWLEDGMENTS

V. REFERENCES

[1] McFarlane DR, Sun J, Golding J, Meakin P, Forsyth M. High conductivity molten salts based on the imide ion. Electrochim Acta. 2000;45:1271–1278.

[2] Armand M, Endres F, MacFarlane DR, Ohno H, Scrosati B. Ionic-liquid Materials for the Electrochemical Challenges of the Future. Nature Mat. 2009;8(8):621–629.

[3] Moreno M, Simonetti E, Appetecchi GB, Carewska M, Montanino M, Kim GT, et al. Ionic Liquid Electrolytes for Safer Lithium Batteries. Journal of The Electrochemical Society. 2016 sep;164(1):A6026–A6031. Available from: https://doi.org/10.1149/2.0051701jes.

[4] Balducci A. Ionic Liquids in Lithium-Ion Batteries. Top Curr Chem. 2017;375(2):20.

[5] Piper DM, Evans T, Leung K, Watkins T, Olson J, Kim SC, et al. Stable silicon-ionic liquid interface for next-generation lithium-ion batteries. Nature Communications. 2015 Feb;6(1):6230. Available from: https://doi.org/10.1038/ncomms7230.

[6] Patel R, Kumari M, Khan AB. Recent Advances in the Application of Ionic Liquids in Protein Stability and Activity: A Review. Appl Biochem Biotechnol. 2014;172:3701–3720.

[7] Smiatek J. Aqueous Ionic Liquids and their Influence on Protein Structures: An Overview on Recent Theoretical and Experimental Insights. J Phys Condens Matter. 2017;29:233001.

[8] Oprzeska-Zingrebe EA, Smiatek J. Aqueous Ionic Liquids in Comparison With Standard Co-solutes. Biophys Rev. 2018:1–16.

[9] Diddens D, Lesch V, Heuer A, Smiatek J. Aqueous Ionic Liquids and Their Influence on Peptide Conformations: Denaturation and Dehydration Mechanisms. Phys Chem Chem Phys. 2017:20430–20440.

[10] Chevrot G, Fileti EE, Chaban VV. Enhanced stability of the model mini-protein in amino acid ionic liquids and their aqueous solutions. J Comput Chem. 2015;36(27):2044–2051.

[11] Weingärtner H, Cabrele C, Herrmann C. How ionic liquids can help to stabilize native proteins. Phys Chem Chem Phys. 2012;14(2):415–426.

[12] Fujita K, MacFarlane DR, Forsyth M. Protein solubilising and stabilising ionic liquids. Chem Commun. 2005;(38):4804–4806.

[13] Zhao H. Protein stabilization and enzyme activation in ionic liquids: specific ion effects. J Chem Technol Biotechnol. 2015;91:25–50.

[14] Silvester DS, Compton RG. Electrochemistry in Room Temperature Ionic Liquids: A Review and Some Possible Applications. Z Phys Chem. 2006;220:1249.

[15] Dommert F, Wendler K, Berger R, Delle Site L, Holm C. Force fields for studying the structure and dynamics of ionic liquids: a critical review of recent developments. ChemPhysChem. 2012;13(7):1625–1637.

[16] Holbrey JD, Reichert WM, Spear SK, Swatloski RP, Turner MB, Visser AE. Ionic liquids as green solvents: progress and prospects. In: ACS Symposium Series. vol. 856; 2003. .

[17] Wang Y, Li H, Han S. A theoretical investigation of the interactions between water molecules and ionic liquids. J Phys Chem B. 2006;110(48):24646–24651.

[18] Schurr JM, Rangel DP, Aragon SR. A contribution to the theory of preferential interaction coefficients. Biophys J. 2005;89(4):2258–2276.

[19] Smith PE. Chemical potential derivatives and preferential interaction parameters in biological systems from Kirkwood-Buff theory. Biophys J. 2006;91(3):849–856.

[20] Smith PE. Chemical potential derivatives and preferential interaction parameters in biological systems from Kirkwood-Buff theory. Biophys J. 2006;91(3):849–856.

[21] Hanke CG, Lynden-Bell RM. A Simulation Study of Water-Dialkylimidazolium Ionic Liquid Mixtures. J Phys Chem B. 2003;107:10873–10878.

[22] Salanne M. Simulations of room temperature ionic liquids: from polarizable to coarse-grained force fields. Phys Chem Chem Phys. 2015;17(22):14270–14279.

[23] Krishnamoorthy AN, Zeman J, Holm C, Smiatek J. Preferential solvation and ion association properties in aqueous dimethyl sulfoxide solutions. Phys Chem Chem Phys. 2016;18(45):31312–31322.

[24] Kobayashi T, Smiatek J, Fyta M. Energetic arguments on the microstructural analysis in ionic liquids. Adv Theory Simul.

[25] Khan I, Kurnia KA, Mutelet F, Pinho SP, Coutinho JA. Probing the interactions between ionic liquids and water: experimental and quantum chemical approach. J Phys Chem B. 2014;118(7):1848–1860.

[26] Quijada-Maldonado E, van der Boogaart S, Lijbers JH, Meindersma GW, de Haan AB. Experimental densities, dynamic viscosities and surface tensions of the ionic liquids series 1-ethyl-3-methylimidazolium acetate and dicyanamide and their binary and ternary mixtures with water and ethanol at T = (298.15 to 343.15 K). J Chem Thermodynamics. 2012;51:51–58.

[27] Courtenay E, Capp M, Anderson C, Record M. Vapor pressure osmometry studies of osmolyte-protein interactions: implications for the action of osmoprotectants in vivo and for the interpretation of "osmotic stress" experiments in vitro. Biochemistry. 2000;39(15):4455–4471.

[28] Fan XH, Chen YP, Su CS. Density and Viscosity Measurements for Binary Mixtures of 1-Ethyl-3-methylimidazolium Tetrafluoroborate ([Emim][BF4]) with Dimethylacetamide, Dimethylformamide, and Dimethyl Sulfoxide. J Chem Eng Data. 2016;61(2):920–927.

[29] Rilo E, Vila J, Pico J, Garcia-Garabal S, Segade L, Varela LM, et al. Electrical conductivity and viscosity of aqueous binary mixtures of 1-alkyl-3-methyl imidazolium tetrafluoroborate at four temperatures. J Chem Eng Data. 2009;55(2):639–644.

[30] Rilo E, Vila J, García-Garabal S, Varela L, Cabeza O. Electrical conductivity of seven binary systems containing 1-ethyl-3-methyl imidazolium alkyl sulfate ionic liquids with water or ethanol at four temperatures. J Phys Chem B. 2013;117(5):1411–1418.

[31] Widegrena JA, Saurerb EM, Marshc KN, Mageea JW. Electrolytic conductivity of four imidazolium-based room-temperature ionic liquids and the effect of a water impurity. J Chem Thermodynamics. 2005;37:569–575.

[32] Yang Z. Hofmeister effects: an explanation for the impact of ionic liquids on biocatalysis. J Biotechnol. 2009;144(1):12–22.

[33] de Souza RF, Padilha JC, Gonçalves RS, Dupont J. Room temperature dialkylimidazolium ionic liquid-based fuel cells. Electrochemistry Communications. 2003;5(8):728–731. Available from: https://www.sciencedirect.com/science/article/pii/S1388248103001735.

[34] Dabirmanesh B, Daneshjou S, Sepahi AA, Ranjbar B, Khavari-Nejad RA, Gill P, et al. Effect of ionic liquids on the structure, stability and activity of two related α-amylases. Int J Biol Macromol. 2011;48(1):93–97.

[35] Vijayaraghavan R, Izgorodin A, Ganesh V, Surianarayanan M, MacFarlane DR. Long-Term Structural and Chemical Stability of DNA in Hydrated Ionic Liquids. Angew Chem Int Ed. 2010;49(9):1631–1633.

[36] Feng G, Jiang X, Qiao R, Kornyshev AA. Water in Ionic Liquids at Electrified Interfaces: The Anatomy of Electrosorption.

ACS Nano. 2014;8(11):11685–11694.

[37] Haberler M, Schröder C, Steinhauser O. Hydrated ionic liquids with and without solute: The influence of water content and protein solutes. J Chem Theo Comput. 2012;8(10):3911–3928.

[38] Seddon KR, Stark A, Torres MJ. Influence of chloride, water, and organic solvents on the physical properties of ionic liquids. Pure Appl Chem. 2000;72(12):2275–2287.

[39] Lesch V, Heuer A, Holm C, Smiatek J. Solvent Effects of 1-Ethyl-3-Methylimidazolium Acetate: Solvation and Dynamic Behavior of Polar and Apolar Solutes. Phys Chem Chem Phys. 2015;17(13):8480–8490.

[40] Lesch V, Heuer A, Holm C, Smiatek J. Properties of Apolar Solutes in Alkyl Imidazolium-Based Ionic Liquids: The Importance of Local Interactions. ChemPhysChem. 2016;17(3):387–394.

[41] Zaera F. Probing Liquid/Solid Interfaces at the Molecular Level. Chem Rev. 2012;112:2920–2986.

[42] Huo F, Liu Z, Wang W. Cosolvent or Antisolvent? A Molecular View of the Interface between Ionic Liquids and Cellulose upon Addition of Another Molecular Solvent. J Phys Chem B. 2013;117:11780–11792.

[43] Rollins JB, Fitchett BD, , Conboy JC. Structure and Orientation of the Imidazolium Cation at the Room-Temperature Ionic Liquid/SiO2 Interface Measured by Sum-Frequency Vibrational Spectroscopy. J Phys Chem B. 2007;111:4990–4999.

[44] Burney PR, Nordwald EM, Hickman K, Kaar JL, Pfaendtner J. Molecular dynamics investigation of the ionic liquid/enzyme interface: Application to engineering enzyme surface charge. Prot Struct Funct Bioinform. 2015;83(4):670–680.

[45] Kobayashi T, Kraus H, Hansen N, Fyta M. Confined Ru-catalysts in a Two-phase Heptane/Ionic Liquid Solution: Modeling Aspects. ChemCatChem. 2021;13(2):739–746. Available from: https://chemistry-europe.onlinelibrary.wiley.com/doi/abs/10.1002/cctc.202001596.

[46] C Nanjundiah SFM, Koch VR. Differential Capacitance Measurements in Solvent-Free Ionic Liquids at Hg and C Interfaces. J Electrochem Soc. 1997;144:3392–3397.

[47] Endres F, Borisenko N, S Z El Abedin RH, Atkin R. The interface ionic liquid(s)/electrode(s): In situ STM and AFM measurements. Faraday Discuss. 2012;154:221–233.

[48] Martin L, Martinez H, Ulldemolins M, Pecquenard B, Cras FL. Evolution of the Si electrode/electrolyte interface in lithium batteries characterized by XPS and AFM techniques: The influence of vinylene carbonate additive. Solid State Ionics. 2012;215:36–44.

[49] Yochelis A, Singh MB, Visoly-Fisher I. Coupling Bulk and Near-Electrode Interfacial Nanostructuring in Ionic Liquids. Chem Mater. 2015;27:4169–4179.

[50] Galiński M, Lewandowski A, Stepniak I. Ionic Liquids as Electrolytes. Electrochim Acta. 2006;51(26):5567–5580.

[51] schröder et al U. Water-induced accelerated ion diffusion : voltammetric studies in 1-methyl-3-[2,6-(S)-dimethylocten-2-yl]imidazolium tetraÑuoroborate, 1-butyl-3-methylimidazolium tetraÑuoroborate and hexaÑuorophosphate ionic liquids. New J Chem. 2000;24:1009–1015.

[52] Rietzler F, Nagengast J, ck HPS, , Maier F. Interface of Ionic Liquids and Carbon: Ultrathin [C1C1Im][Tf2N] Films on Graphite and Graphene. J Phys Chem C. 2015;119:28068–28076.

[53] Bi S, Wang R, Liu S, Yan J, Mao B, Kornyshev AA, et al. Minimizing the electrosorption of water from humid ionic liquids on electrodes. Nature Communications. 2018 Dec;9(1):5222. Available from: https://doi.org/10.1038/s41467-018-07674-0.

[54] Kobayashi T, Kemna A, Fyta M, Braunschweig B, Smiatek J. Aqueous Mixtures of Room-Temperature Ionic Liquids: Entropy-Driven Accumulation of Water Molecules at Interfaces. J Phys Chem C. 2019;123(22):13795–13803.

[55] Chapman DL. LI. A contribution to the theory of electrocapillarity. The London, Edinburgh, and Dublin Philosophical Magazine and Journal of Science. 1913;25:475–481.

[56] Kornyshev AA. Double-Layer in Ionic Liquids: Paradigm Change? J Phys Chem B. 2007;111:5545–5557.

[57] Zachary A H Goodwin AAK. Underscreening, overscreening and double-layer capacitance. Electrochemistry Communications. 2017;82:129–133.

[58] Bazant MZ, Storey BD, Kornyshev AA. Double Layer in Ionic Liquids: Overscreening versus Crowding. Phys Rev Lett. 2011 Jan;106:046102. Available from: https://link.aps.org/doi/10.1103/PhysRevLett.106.046102.

[59] Stillinger FH, Kirkwood JG. Theory of the Diffuse Double Layer. The Journal of Chemical Physics. 1960;33(5):1282–1290. Available from: https://doi.org/10.1063/1.1731401.

[60] Fedorov MV, Kornyshev AA. Towards understanding the structure and capacitance of electrical double layer in ionic liquids. Electrochimica Acta. 2008;53(23):6835–6840. EXPLORING FRONTIERS OF ELECTROCHEMISTRY Selection of papers from the 58th Annual Meeting of the International Society of Electrochemistry 10-14 September 2007, Banff, Canada. Available from: https://www.sciencedirect.com/science/article/pii/S0013468608002478.

[61] Jitvisate M, Seddon JRT. Near-Wall Molecular Ordering of Dilute Ionic Liquids. The Journal of Physical Chemistry C. 2017;121(34):18593–18597. PMID: 28883896. Available from: https://doi.org/10.1021/acs.jpcc.7b04843.

[62] Horn RG, Evans DF, Ninham BW. Double-layer and solvation forces measured in a molten salt and its mixtures with water. The Journal of Physical Chemistry. 1988;92(12):3531–3537. Available from: https://doi.org/10.1021/j100323a042.

[63] Atkin R, Warr GG. Structure in Confined Room-Temperature Ionic Liquids. The Journal of Physical Chemistry C. 2007;111(13):5162–5168. Available from: https://doi.org/10.1021/jp067420g.

[64] Chu M, Miller M, Dutta P. Crowding and Anomalous Capacitance at an Electrode–Ionic Liquid Interface Observed Using Operando X-ray Scattering. ACS Central Science. 2016;2(3):175–180. PMID: 27163044. Available from: https://doi.org/10.1021/acscentsci.6b00014.

[65] Jurado LA, Espinosa-Marzal RM. Insight into the Electrical Double Layer of an Ionic Liquid on Graphene. Scientific Reports. 2017 Jun;7(1):4225. Available from: https://doi.org/10.1038/s41598-017-04576-x.

[66] Begić S, Chen F, Jónsson E, Forsyth M. Overscreening and crowding in electrochemical ionic liquid systems. Phys Rev Materials. 2019 Sep;3:095801. Available from: https://link.aps.org/doi/10.1103/PhysRevMaterials.3.095801.

[67] Torrie GM, Valleau JP. Electrical double layers. I. Monte Carlo study of a uniformly charged surface. The Journal of Chemical Physics. 1980;73(11):5807–5816. Available from: https://doi.org/10.1063/1.440065.

[68] Merlet C, Péan C, Rotenberg B, Madden PA, Simon P, Salanne M. Simulating Supercapacitors: Can We Model Electrodes As Constant Charge Surfaces? The Journal of Physical Chemistry Letters. 2013;4(2):264–268. PMID: 26283432. Available from: https://doi.org/10.1021/jz3019226.

[69] Van Der Spoel D, Lindahl E, Hess B, Groenhof G, Mark AE, Berendsen HJ. GROMACS: fast, flexible, and free. J Comput Chem. 2005;26(16):1701–1718.

[70] Pronk S, Páll S, Schulz R, Larsson P, Bjelkmar P, Apostolov R, et al. GROMACS 4.5: A High-throughput and Highly Parallel Open Source Molecular Simulation Toolkit. Bioinformatics. 2013;29(7):845.

[71] Abraham MJ, Murtola T, Schulz R, Páll S, Smith JC, Hess B, et al. GROMACS: High Performance Molecular Simulations Through Multi-Level Parallelism from Laptops to Supercomputers. SoftwareX. 2015;1:19–25.

[72] Jorgensen WL, Maxwell DS, Tirado-Rives J. Development and Testing of the OPLS All-Atom Force Field on Conformational Energetics and Properties of Organic Liquids. J Am Chem Soc. 1996;118(45):11225–11236.

[73] Canongia Lopes JN, Deschamps J, Pádua AA. Modeling Ionic Liquids Using a Systematic All-Atom Force Field. J Phys Chem B. 2004;108(6):2038–2047.

[74] Sambasivarao SV, Acevedo O. Development of OPLS-AA Force Field Parameters for 68 Unique Ionic Liquids. J Chem Theory Comput. 2009;5(4):1038–1050.

[75] Caleman C, van Maaren PJ, Hong M, Hub JS, Costa LT, van der Spoel D. Force Field Benchmark of Organic Liquids: Density, Enthalpy of Vaporization, Heat Capacities, Surface Tension, Isothermal Compressibility, Volumetric Expansion Coefficient, and Dielectric Constant. J Chem Theory Comput. 2012;8(1):61–74.

[76] Berendsen H, Grigera J, Straatsma T. The Missing Term in Effective Pair Potentials. J Phys Chem. 1987;91(24):6269–6271.

[77] Kobayashi T, Reid JE, Shimizu S, Fyta M, Smiatek J. The Properties of Residual Water Molecules in Ionic Liquids: A Comparison Between Direct and Inverse Kirkwood–Buff Approaches. Phys Chem Chem Phys. 2017;19:18924–18937.

[78] Bussi G, Donadio D, Parrinello M. Canonical sampling through velocity rescaling. J Chem Phys. 2007;126(1):014101.

[79] Darden T, York D, Pedersen L. Particle mesh Ewald: An N log (N) method for Ewald sums in large systems. J Chem Phys. 1993;98(12):10089–10092.

[80] Essmann U, Perera L, Berkowitz ML, Darden T, Lee H, Pedersen LG. A smooth particle mesh Ewald method. J Chem Phys. 1995;103(19):8577–8593.

[81] Hess B, Bekker H, Berendsen HJC, Fraaije JGEM. LINCS: A linear constraint solver for molecular simulations. J Comput Chem. 1997;18:1463–1472.

[82] Martínez L, Andrade R, Birgin EG, Martínez JM. PACKMOL: a package for building initial configurations for molecular dynamics simulations. J Comput Chem. 2009;30(13):2157–2164.

[83] Yeh IC, Berkowitz ML. Ewald summation for systems with slab geometry. J Chem Phys. 1999;111(7):11780–11792.

[84] Parrinello M, Rahman A. Polymorphic Transitions in Single Crystals: A New Molecular Dynamics Method. J Appl Phys. 1981;52(12):7182–7190.

[85] Jitvisate M, Seddon JRT. Local Structure and Flow Properties of Ionic Liquids on Charged and Inert Substrates. J Phys Chem C. 2016;120:4860–4865.

[86] Gebbie MA, Valtiner M, Banquy X, Fox ET, Henderson WA, Israelachvili JN. Ionic liquids behave as dilute electrolyte solutions. Proc Natl Acad Sci USA. 2013;110(24):9674–9679.

[87] Bondi A. van der Waals Volumes and Radii. J Phys Chem. 1964;68:441–451.

[88] Płowaś I, Świergiel J, Jadżyn J. Relative Static Permittivity of Dimethyl Sulfoxide + Water Mixtures. Journal of Chemical & Engineering Data. 2013;58(6):1741–1746. Available from: https://doi.org/10.1021/je400149j.

[89] Neumann M. Dipole moment fluctuation formulas in computer simulations of polar systems. Molecular Physics. 1983;50(4):841–858. Available from: https://doi.org/10.1080/00268978300102721.

[90] NIST Computational Chemistry Comparison and Benchmark Database NIST Standard Reference Database Number 101 Release 21, August 2020, Editor: Russell D. Johnson III;. DOI:10.18434/T47C7Z. http://cccbdb.nist.gov/.

[91] Miranda-Quintana RA, Smiatek J. Beneficial properties of solvents and ions for lithium ion and post-lithium ion batteries: Implications from charge transfer models. Electrochim Acta. 2021;384:138418.

[92] Miranda-Quintana RA, Smiatek J. Specific Ion Effects in Different Media: Current Status and Future Challenges. J Phys Chem B. 2021;125:13840–13849.

[93] Miranda-Quintana RA, Smiatek J. Theoretical Insights into Specific Ion Effects and Strong-Weak Acid-Base Rules for Ions in Solution: Deriving the Law of Matching Solvent Affinities from First Principles. ChemPhysChem. 2020;21(23):2605–2617.